# Clouds at the tropical tropopause: A case study during the APE-THESEO campaign over the western Indian Ocean

Vincenzo Santacesaria,[1,2] Roberto Carla,[1] Robert MacKenzie,[3] Alberto Adriani,[4] Francesco Cairo,[4] Guido Didonfrancesco,[4,5] Christoph Kiemle,[6] Gianluca Redaelli,[7] Jürgen Beuermann,[8] Cornelius Schiller,[8] Thomas Peter,[9] Beiping Luo,[9] Heini Wernli,[9] Fabrizio Ravegnani,[10] Alexey Ulanovsky,[11] Vladimir Yushkov,[11] Nikolay Sitnikov,[11] Stefano Balestri,[12] and Leopoldo Stefanutti[13]

Received 5 February 2002; revised 10 May 2002; accepted 22 May 2002; published 18 January 2003.

[1] In this paper, we report a detailed description of a thin cirrus at the tropopause above a cumulonimbus (Cb) convective cluster observed during the Airborne Platform for Earth Observation–Third European Stratospheric Experiment for Ozone (APE-THESEO) campaign in February–March 1999 in the western Indian Ocean. The thin cirrus (Ci) has an optical depth at 532 nm below 0.1, with extended subvisible stretches, and is located directly below the tropopause, which was supersaturated with respect to ice. A direct comparison between the optical depth retrieved by Meteosat and that obtained by means of the hygrometers installed on the M55-Geophysica aircraft is discussed showing discrepancies ranging from 10 to 20%. Combining satellite and aircraft data, we show that the observed Ci is not due to cirrus outflow from Cb anvils. In the absence of any deeply convective clouds reaching altitudes above 15 km, we propose a possible mechanism of Ci formation based on a net mesoscale transport of water vapor from altitudes above 16 km to the tropopause region around 18 km. This transport could be driven by the critical layer and turbulence induced by gravity waves that could have been generated by lower level Cb cluster activity. The proposed mechanism for high-altitude Ci formation corroborates the new paradigm of a tropical tropopause layer (TTL) or ''substratosphere,'' several kilometers thick, which is decoupled from the convection-dominated lower troposphere. *INDEX TERMS:* 0320 Atmospheric Composition and Structure: Cloud physics and chemistry; 0368 Atmospheric Composition and Structure: Troposphere—constituent transport and chemistry; 0394 Atmospheric Composition and Structure: Instruments and techniques; *KEYWORDS:* thin tropical cirrus, APE-THESEO campaign, tropical tropopause layer (TTL), convective system

**Citation:** Santacesaria, V., et al., Clouds at the tropical tropopause: A case study during the APE-THESEO campaign over the western Indian Ocean, *J. Geophys. Res.*, *108*(D2), 4044, doi:10.1029/2002JD002166, 2003.

## 1. Introduction

[2] Past observations have revealed very low water vapor concentrations in the lower stratosphere over tropical regions [*Holton et al.*, 1995; *Tuck et al.*, 1997]. The Brewer-Dobson theory for stratospheric circulation [*Brewer*, 1949] suggests that the upward branch of the circulation is located in the tropics. The cold temperatures encountered by the air masses upon crossing the tropical tropopause region limits the water vapor content with which they enter the stratosphere. Recently, the special character of the altitude range a few kilometers below the tropical tropopause, which is only rarely penetrated by deep convection, has been emphasized by naming this region ''substratosphere'' [*Thuburn and Craig*, 2000] or tropical tropopause layer (TTL) [*Sherwood and Dessler*, 2000].

[1]Istituto di Fisica Applicata ''Nello Carrara,'' Consiglio Nazionale delle Richerche, Florence, Italy.
[2]Now at Advanced Computer System SpA, Rome, Italy.
[3]Environmental Science Department, Lancaster University, Lancaster, UK.
[4]Istituto di Scienze dell'Atmosfera e del Clima, Consiglio Nazionale delle Richerche, Rome, Italy.
[5]Ente per le Nuove Tecnologie, l'Energia e l'Ambiente-Clim, Rome, Italy.
[6]Deutsches Zentrum für Luft- und Raumfahrt, Oberpfaffenhofen, Wessling, Germany.
[7]Dipartimento di Fisica, Universita' Dell'Aquila, Coppito, L'Aquila, Italy.
[8]Forschungszentrum Jülich, Jülich, Germany.
[9]Institute for Atmospheric and Climate Science, Swiss Federal Institute of Technology (ETH), Zurich, Switzerland.
[10]Istituto di Scienze dell'Atmosfera e del Clima, Consiglio Nazionale delle Richerche, Bologna, Italy.
[11]Central Aerological Observatory, Dolgoprudny, Russia.
[12]Airborne Platform for Earth Observation srl, Florence, Italy.
[13]Geophysica-Gruppo Europeo di Interesse Economico, Florence, Italy.


0148-0227/03/2002JD002166

[3] Nevertheless, the low water vapor mixing ratios of ≈2 ppmv observed in the lowermost tropical stratosphere cannot be explained in terms of the average value of tropical tropopause temperatures observed globally. Little is known about the drying mechanisms at work. Three distinctive mechanisms have been suggested: (1) slow upwelling that dries air through large-scale formation of ice particles [*Brewer*, 1949; *Newell and Gould Stewart*, 1981] in visible or possibly subvisible cirri, (2) convective overshooting with extreme cooling followed by dehydration due to sedimenting ice particles and subsequent mixing of the dehydrated air into the stratosphere [*Danielsen*, 1982], and (3) wave-induced cirrus cloud formation, either below the tropopause, for example by Kelvin wave forcing [*Boehm and Verlinde*, 2000], or above the tropopause, for example in buoyancy waves leading to dehydration in situ in the lower stratosphere [*Potter and Holton*, 1995].

[4] *Newell and Gould Stewart* [1981] suggested that air could enter the stratosphere only over particularly cold tropical areas (named 'stratospheric fountains'), in which a sufficient amount of tropospheric air crossing the cold tropopause could explain the water content observed in the stratosphere.

[5] Another mechanism, that could be responsible for the dehydration of the tropospheric air masses entering the stratosphere, was suggested by *Danielsen* [1982], who postulated that cumulonimbus anvils, when penetrating the stratosphere, are destabilized by longwave heating below the cirrus anvil and radiative cooling above it. This allows for the growth of large ice particles and the removal of condensed phase water from the lower stratosphere by sedimentation. One essential condition for the presence of such a mechanism is that Cbs must reach the local tropopause in order to have such an impact on the lower stratosphere.

[6] *Potter and Holton* [1995] postulated that tropical convection need not penetrate the tropopause in order to act on the water content in the lower stratosphere. By using a model, which simulates the development of convection over the northwest coast of Borneo, they concluded that thin cirrus clouds forming in the lower tropical stratosphere caused by upwelling buoyancy waves might contribute to the observed water vapor minimum. However, conclusive experimental evidence for the existence of ice particles or even cirrus clouds in the lower tropical stratosphere is still missing. On the other hand, there is evidence from previous airborne campaigns for buoyancy waves, which are associated with strong convection and are a necessary prerequisite for the hypothesis of *Potter and Holton* [1995]. *Pfister et al.* [1993] reported observations performed during the STEP campaign with the ER-2. In particular, they found oscillations of the temperature of the order of 5 K when flying above mesoscale convection. The relationship among different meteorological parameters (T, u, w) suggests that these oscillations may be ascribed to gravity waves propagating upwards. Furthermore, by using radiosonde observations, *Tsuda et al.* [1994] found, over Indonesia, where strong convection is often present, that temperature fluctuations were around 2 K in the troposphere and could exceed 3 K in the stratosphere. Also in this case, the oscillations can be ascribed to gravity waves propagating upwards, associated with the Cbs below.

[7] By means of microphysical modeling, *Jensen et al.* [1996a] argued that the crystals would not grow larger than 10 microns in ice clouds forming in buoyancy waves, and that sedimenting ice therefore caused only little dehydration. On the other hand, they also showed that in clouds associated with large-scale upwelling motion the crystals could grow to larger sizes and have more time for sedimentation leading to dehydration of the tropopause region and hence of the lower stratosphere. Spaceborne lidar observations [*Winker and Trepte*, 1998] and limb viewing measurements confirm that extended thin cloud structures at the tropopause are quite frequent in the tropical regions. The average geometric thickness of these cirrus (Ci), as determined by lidars located in the tropical area, is around 600 m with an optical thickness of 0.008–0.01 [*Platt et al.*, 1998; *Nee et al.*, 1998]. Cirrus clouds with an optical thickness below the limit of 0.03 are categorized as subvisible [*Sassen and Cho*, 1992], as they cannot be observed by the naked eye. This complicates their analysis and detection, which can only be achieved by lidar technology.

[8] Using results coming from various aircraft campaigns (CEPEX, TOGA COARE) and satellite observations, *McFarquhar et al.* [2000] concluded that despite their extreme thinness the subvisible clouds have a non-negligible effect on the radiative budget of the tropical region. Furthermore, they may affect the upper tropospheric vertical motions and the water vapor content of the lower stratosphere.

[9] Using lidar [*Browell et al.*, 1983] observations, *Pfister et al.* [2001] subdivided the subvisible clouds (SVCs) in the tropics into two main categories according to their lidar backscattering ratio and the altitude at which they are located. The first class, SVC I, is characterized by a maximum backscatter ratio, at 603 nm, of 4–5 or even higher, and are located below the tropical tropopause with a maximum potential temperature not higher than 380 K. They indicated that this class of SVC is related to strong persistent convection present in the observation areas. Class II SVCs are represented by thinner clouds with a smaller scattering ratio than class I, and are located at higher altitude around 390 K. Speculations based on the thermal history indicate that these clouds may be generated by gravity or inertio-gravity waves.

[10] One of the major issues related to the thin clouds observed at the tropical tropopause concerns their mechanism of formation and maintenance. In this study we describe a novel data set based on in situ and remote measurements from two research aircraft and Meteosat 5 of a thin cirrus over the tropical Indian Ocean.

[11] Even though the collected data set is still too limited, objective of this study is to use it in order to speculate about the roles of different physical processes in the formation of tropical thin cirrus clouds, on the base of the adaptability of existing theories with the present data set.

## 2. APE-THESEO Campaign

[12] During February and March 1999 the APE-THESEO campaign took place as the first European high-altitude airborne tropical experiment (L. Stefanutti et al., The APE-THESEO tropical campaign, submitted to *Journal of Atmospheric Chemistry*, 2002). Two aircraft, the M-55 Geophysica

(which can fly up to 22 km) and the DLR Falcon, performed combined flights over the western Indian Ocean.

[13] During the campaign, convective activity was generally not strong enough to reach the tropopause. The satellite data show that anvils associated with Cbs on the average remained a couple of km below the local tropopause (with the exception of the last four days of the campaign). This is in accord with our in situ and lidar measurements of deeply convective systems. Conversely, the measurements show thin clouds at the tropopause, as well as a surprisingly cold and dry tropopause (A. R. MacKenzie et al., manuscript in preparation, 2002).

[14] Amongst the most remarkable findings of this campaign was the detection of ultrathin tropical tropopause clouds (UTTCs) with geometrical thicknesses around 200–300 m and optical depths around $10^{-4}$. These distinct layers appear to be long lasting and geographically very extended; see B. P. Luo et al. (Dehydration potential of ultrathin clouds at the tropical tropopause, submitted to *Geophysical Research Letters*, 2002) (hereinafter referred to as Luo et al., submitted manuscript, 2002) for details. Here we do not report on UTTCs but on thicker SVCs that might lead to UTTC formation upon evaporation.

### 2.1. In Situ Measurements

[15] During APE-THESEO, the Geophysica carried a comprehensive scientific payload with in situ sensors to measure meteorological parameters, water vapor, ozone, and trace gases, further with an in situ size-resolving aerosol counter as well as with two upward looking aerosol lidar systems. The current analysis relies mostly on data from the following in situ instruments on board Geophysica: data from MAS [*Adriani et al.*, 1999], a multiwavelength aerosol scatterometer, which operated at 532 nm during the tropical campaign and allows to measure both, the parallel and the perpendicular (depolarized) components of the backscattered light; data from FISH [*Zöger et al.*, 1999] and from FLASH [*Merkulov and Yushkov*, 1999], two Ly-$\alpha$ fluorescence hygrometers measuring the total and the gas phase content of $H_2O$, respectively; data from FOZAN, a chemiluminescent ozone sensor that detects fast ozone variations [*Yushkov et al.*, 1999], which are used to distinguish tropospheric from stratospheric air. The in situ payload includes also a modified FSSP-300 optical particle detection instrument covering a particle diameter size ranging from 0.4 to 23 $\mu$m. Unfortunately, this instrument did not work during the first flight, but it collected several measurements in following flights [*Thomas et al.*, 2002].

### 2.2. Remote Sensing of Clouds by Lidar

[16] The research aircraft Falcon of the German Aerospace Center (DLR) carried the 4-wavelength aerosol and ozone lidar OLEX (Ozone Lidar Experiment) in zenith-viewing mode [*Wirth and Renger*, 1996]. OLEX provided two-dimensional vertical cross sections of visible and subvisible cirrus cloud backscatter ratios at 354, 532 and 1064 nm, of the depolarization ratio at 532 nm, and of stratospheric ozone. The backscatter ratio is defined as the ratio of total (aerosol plus air molecular) backscatter coefficient divided by pure air molecular backscatter coefficient. The OLEX on board of the Falcon provided unprecedented new views of Ci and SVCs in the TTL (cf. Luo et al., submitted manuscript, 2002). Besides following its own research goals, the Falcon served as path-finding aircraft for the Geophysica. Both aircraft can fly with the same speed at their respective altitudes, allowing simultaneous detailed in situ and remote measurements of the same clouds.

### 2.3. Satellite Support

[17] The campaign took place simultaneously with the INDOEX (Indian Ocean Experiment) intensive field phase (A. Clarke et al., An overview of the C-130 flight missions and measurements during INDOEX, submitted to *Journal of Geophysical Research*, 2001), which was supported by Meteosat 5 cloud images in order to provide information on convective cloud activity in the area. For this purpose Meteosat 5 was relocated to 63°E, i.e., directly above the Indian Ocean, and APE-THESEO profited from this relocation. The satellite radiometer acquires images simultaneously in three spectral ranges: in the visible (0.5–0.9 $\mu$m), thermal infrared (IR) (10.5–12.5 $\mu$m), and water vapor (WV) (5.7–7.1 $\mu$m). The acquisition frequencies of 30 minutes with total coverage and high spatial resolution of 5 km at the equator are adequate for the observation of fast atmospheric processes in a large oceanic region.

### 2.4. Case Study

[18] In this paper we describe specifically the flight of 19 February when extended thin cirrus with optical depths between 0.01 and 0.09 was observed. The cirrus was located close to the tropopause above, but clearly detached from an area of moderate Cb activity, similar to visual observations from aircraft by *Harris-Hobbs et al.* [1990]. The cloud is characterized by a relatively high backscattering ratio and optical depth. Its high altitude does not allow the cloud to be classified according to the scheme proposed by *Pfister et al.* [2001], who considered Ci as an anvil outflow. Conversely, these clouds may play a role in the formation of UTTCs (Luo et al., submitted manuscript, 2002).

## 3. Case Study of Flight on 19 February 1999

[19] In Figure 1, the Geophysica flight path is shown on the corresponding IR Meteosat 5 image. The Falcon flew precisely the same path 30 to 60 minutes ahead of the Geophysica in order to serve as pathfinder and to provide the Geophysica pilot with cloud altitude information.

### 3.1. Meteorological Characterization

[20] The color code used in Figure 1 represents cloud top brightness temperature. Two different convective regions can be identified. The more intense and extensive system is located to the west and southwest of the Seychelles, and has a cloud top temperature around −65°C, corresponding to roughly 2 km below the tropopause (measured along the flight path). Another system is located to the north of the Seychelles, characterized by a cluster of isolated Cbs with cloud top brightness temperatures higher than −50°C. It should be noted that these temperatures are only estimates. The brightness temperature in the IR images corresponds to the actual temperature only for opaque clouds, as is appropriate for Cbs. For thin cirrus clouds, however, the weak emissivity would have to be taken into account in the

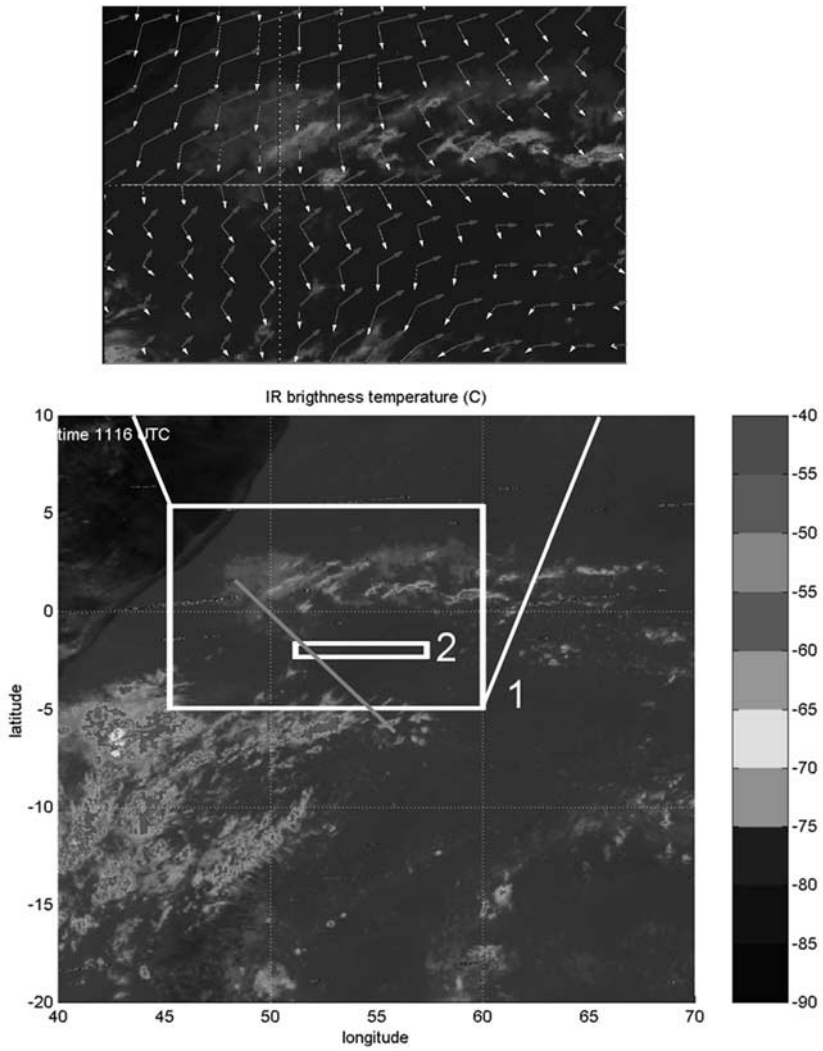


**Figure 1.** IR brightness temperature image acquired by Meteosat 5 during the APE-THESEO flight on 19 February 1999 from the Seychelles towards Mogadishu (the coastline of Somalia is visible in the upper left corner). The red line indicates the flight path of the aircraft, and the white box (box 1) indicates a region with high cirrus close to the tropopause. Included in this box is a second white box (box 2) that is considered in the analysis reported in Figure 6. The inset shows the wind field at 200 mbar (red) and 100 mbar (blue); the direction of the anvils outflow is aligned to the wind field at 200 mbar. See color version of this figure at back of this issue.

derivation of the actual temperature. This will be discussed later in the paper and we return to this complication below.

[21] The flight path adopted on that day took the two aircraft in a southeasterly direction towards the region with isolated and moderate Cbs. Within the area indicated by the white square in Figure 1, the Geophysica made direct observations of the local tropopause. Figure 2 shows the temperature profile measured on board of the Geophysica measured during various dives and ascents. The tropopause region was very cold, with a minimum temperature ranging from $-87$ to $-90$°C. The cold-point tropopause is located around 18.2 km. This tropopause is unexpectedly high for the western Indian Ocean, higher than observed during most other flights performed during APE-THESEO (A. R. MacKenzie et al., manuscript in preparation, 2002). The high altitude of the tropopause may be a consequence of the convection present in the area (Luo et al., submitted manuscript, 2002). In the tropics, cumulus convection may be associated with anomalously high tropopauses, as observed during the MONEX campaign [*Johnson and Kriete*, 1982].

[22] Figure 3 shows the wind speed and direction diagram (hodogram) retrieved by the ECMWF analysis averaged inside the boxed area (numbered 1) indicated in Figure 1. At high altitudes, the wind was northeasterly with a speed of around 14 m/s. At lower altitudes the wind speed decreases. The wind direction for altitudes below 14 km (140 mbar) was southwesterly, and remains in that sector down to 9 km (300 mbar). Below 9 km the winds turn northeasterly again.

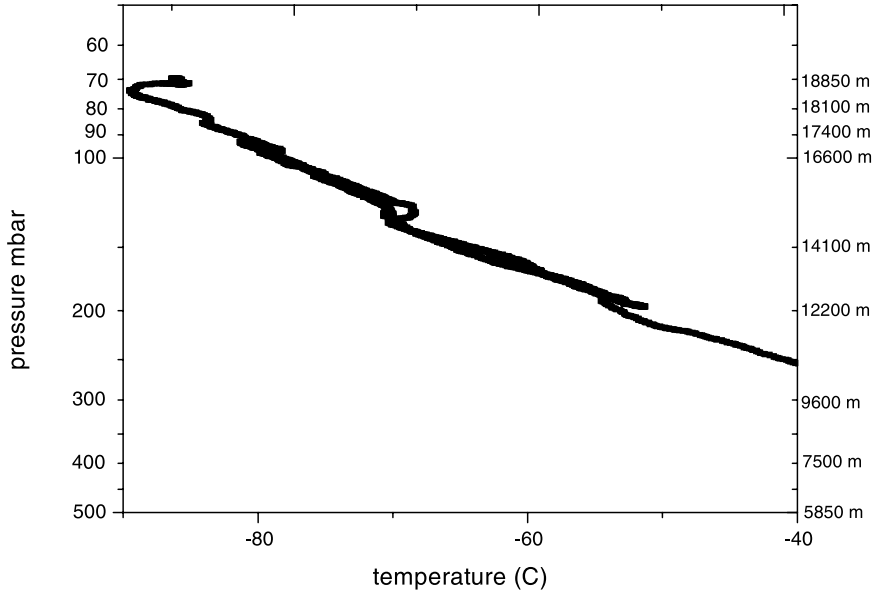


**Figure 2.** Temperature profile obtained by the Geophysica during the flight, showing a very high tropopause with minimum temperatures of −90°C.

[23] This horizontal shear is very useful information in the interpretation of the satellite images, as high clouds at different altitudes are advected in different directions, and following their direction allows us to identify their altitude in a better way than is possible from the brightness temperatures.

[24] In the inset of Figure 1 we show in detail a section of the Meteosat 5 image, focusing on the region where the Cb clusters were present. By assuming the emissivity to be unity, the top of these Cbs, with a brightness temperature around −55°C, corresponds to an altitude of roughly 13 km between (200 140 mbar) (see Figure 1). In Figure 1, the Meteosat picture is combined with the wind field at 200 mbar and 100 mbar retrieved from the ECMWF analysis. This reveals that the anvil outflows associated with the highest Cbs (red and green colors in Figure 1) were directed to the northeast, according to the mean wind direction at that altitude (see winds direction at 200–140 mbar in the hodogram in Figure 3). On the other hand the Cbs pattern is inconsistent with the direction of the winds at higher altitude, like for instance those at 100 mbar reported in Figure 1 (see the hodogram in Figure 3 for other high-level winds). It is therefore evident (brightness temperature and wind field) that the outflow of the Cb cluster activity was located at an altitude not above 200–140 mbar, i.e., some kilometers below the altitude of the local tropopause. Overshooting of the strongest Cbs to higher altitudes in the TTL region cannot be excluded. Closer inspection reveals that besides the Cbs and their anvils, there is a stratiform low-altitude cloud system located below 500 mbar in the same region, represented by a greyish area in Figure 1.

### 3.2. In Situ and Remote Particle and Gas Measurements

[25] The cirrus layer was crossed several times during the outward and inward flight legs, as reported in Figure 4. Close correspondence is shown between in situ observations from MAS and the remote sensing by the Falcon lidar, which observed the cirrus cloud to be close to the tropopause around 18 km with a maximum thickness of the order of 1 km and a maximum backscatter ratio around 10 at 532 nm. Figure 4a shows the Falcon measurements at 532 nm together with the Geophysica flight altitude as obtained from the onboard GPS (black curve). The Geophysica was maneuvered into the cirrus deck, which is hardly visible for the pilot, according to the instructions given by the lidar scientists on board of the Falcon. Figure 4b shows the MAS measurement performed during the inward leg at the same latitudes. The in situ backscattering observation confirmed the general geometric and optical characteristics of the cloud retrieved by remote measurement. The delay of 2500 sec of the Geophysica flying after the Falcon has to be taken into account when comparing the two measurements. This delay

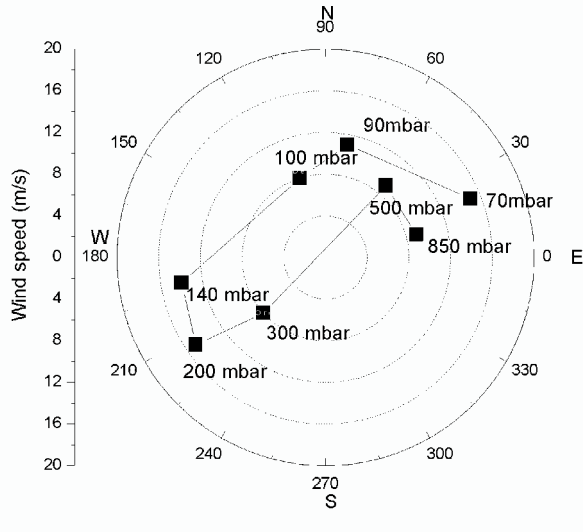


**Figure 3.** Hodogram using ECMWF data analysis showing the average winds in the boxed region indicated in Figure 1.

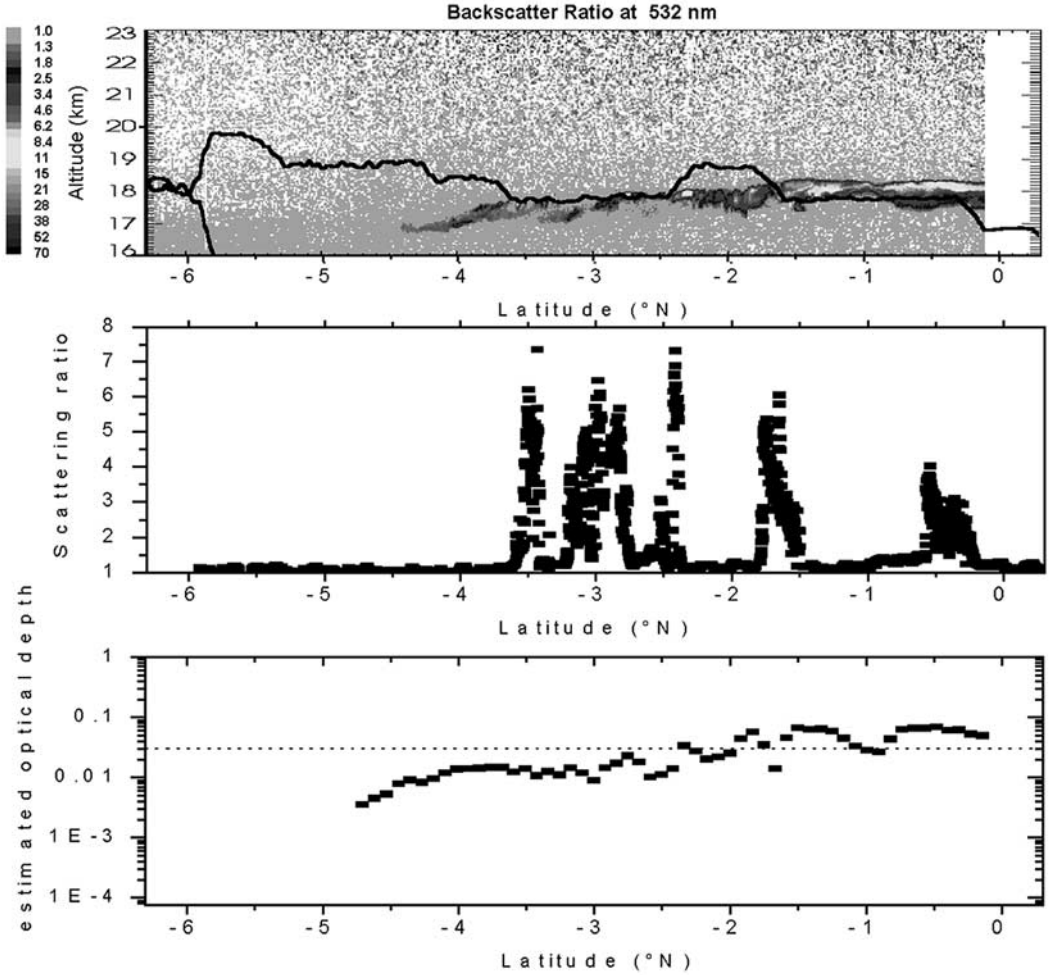


**Figure 4.** Comparison between aerosol backscatter ratios measured by OLEX on the Falcon (a) and by MAS on the Geophysica (b). The Geophysica flight path is shown as a black curve in Figure 4a. Some discrepancies can be ascribed to the different times of the measurements (40 min delay of Geophysica). Estimated value of the optical depth as a function of the latitude is reported in Figure 4c using an extinction/backscattering ratio of 125 sr (see text for details). The dashed line represents the threshold for subvisible clouds as indicated by *Sassen and Cho* [1992].

could explain some of the discrepancies observed between both data sets, as it is likely that the cloud was not quite stationary. In any case, the comparison reveals good agreement between the measurements. The layer was crossed only once in full width during the inward flight leg, while the other observations correspond to partial crossings from below (i.e., for latitudes north 1.5°S) and from above (i.e., for latitudes south of 2.5°S). Figure 4c reports the estimated optical depth at 532 nm using the vertically integrated lidar data and a value of 125 sr for the extinction/backscatter ratio (more details are reported in the following section).

[26] Comparing this figure with the temperature profile reported in Figure 2 reveals that the strong inversion present at the local tropopause coincides with the top of this cloud layer. The thickness, the scattering ratio, and the top altitude of the cloud structure decreased towards the south. This can possibly be ascribed to older parts of the cloud, which sediment and evaporate at lower altitudes.

[27] Figure 5 shows some of the Geophysica in situ measurements as function of time: the particle backscatter ratio from MAS, the cloud water content from FISH, the flight altitude, and the latitude. The inlet of FISH oversamples particles, enhancing the water signal from particulate matter by about a factor of 5. This is corrected for in Figure 5. The maximum backscatter ratios measured by MAS during each cloud encounter was 6–8, while the maximum water mixing ratios in the condensed phase derived from the FISH measurement were around 1.8–2.2 ppmv (with spikes up to 3–4 ppmv $H_2O$). In the latitude range between 0 and 2°S, the base and the top of the cirrus cloud were located between 17.5 and 18.5 km. The cloud layer is not uniform, as shown by the data between 43000 s and 45000 s UTC in Figure 5.

## 4. Optical Depth Estimates From Meteosat Observations

[28] The aircraft measurements provide information that allows us to refine our analysis of the Meteosat 5 images. We use the method reported by *Ackerman et al.* [1988] in

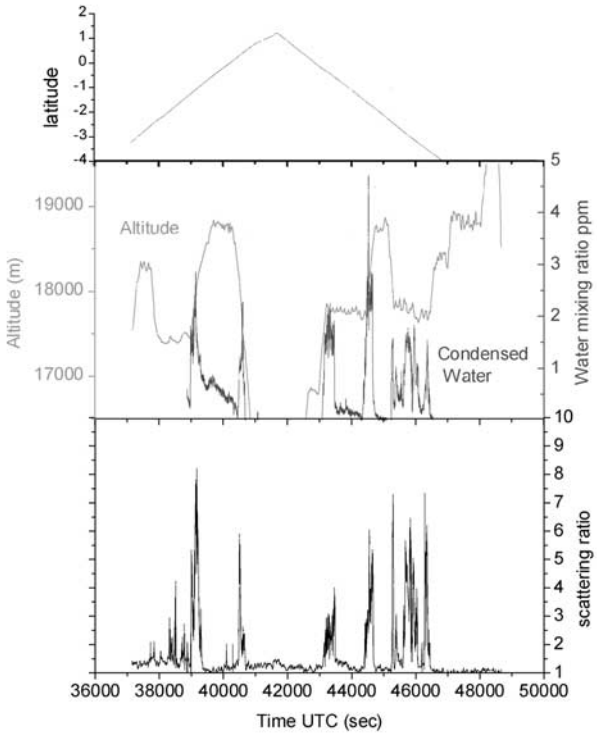


**Figure 5.** Latitudes covered (upper panel) and in situ measurements performed by the Geophysica (middle and lower panels) during the flight on 19 February 1999. Lower panel: aerosol backscattering ratio at 532 nm from MAS. Middle panel: condensed phase water mixing ratio (after subtraction of gas phase mixing ratio) and GPS flight altitude. See color version of this figure at back of this issue.

order to calculate the cloud optical depth in the presence of thin cirrus clouds. From this we estimate the ice water content, using the thermal channel data of Meteosat 5.

### 4.1. Meteosat-FISH Comparison

[29] Assuming that no midlevel clouds were present between the sea surface and the cirrus layer, the IR thermal radiance measured by the radiometer on board of Meteosat can be expressed as:

$$B_o = B_s(1-\varepsilon) + B_c\varepsilon + B_s\delta_s(\tau) - B_c\delta_c(\tau); \quad (1)$$

$B_s$ represents the radiance emitted by the surface below the cloud, which we assume to be the highest radiance observed around the region of interest; $B_c$ is the blackbody cloud radiance calculated assuming the cloud isothermal temperature to be equal to $T_c$; $\tau$ is the cloud optical depth; and $\varepsilon$ is the cloud absorption emissivity which is related to $\tau$ by the following expression:

$$\varepsilon = 1 - e^{-\tau} \quad (2)$$

This expression is very approximate, because we assumed that inside the cloud layer the temperature was isothermal.

[30] In equation (1), the first two terms represent the transmission and the thermal emission through the cloud treated as a non-scattering medium. Corrections due to the scattering are represented by the third and the fourth terms ($B_s\delta_s(\tau)$; $B_c\delta_c(\tau)$), which are a function among others of the single scattering albedo ($\varpi$) and the asymmetry factor (g) [cf. *Ackerman et al.*, 1988]. We use values of $\varpi = 0.5$ and $g = 0.85$ assuming the particles to be cirrus ice crystals, as has been suggested by *Liou* [1974]. From equation (1), given the values of $B_o$ and $B_s$ and the temperature of the cloud layer $T_c$ (measured directly by the aircraft), the optical depth of the cloud can be retrieved. It is worthwhile to observe that, due to the small value of the optical depth reported in this study, neglecting the terms for the correction for scattering the induced error in the estimated value of the optical depth is about only 5%.

[31] Another issue concerns the calibration of the IR channel of the Meteosat 5. In this case we have estimated than an error up to 50% in the value of the calibration coefficient will induce an error in the estimated optical depth of less than 3%. This implies that the estimated optical depth is not very sensitive to the calibration coefficient. That is probably due to the fact that assuming the same coefficient for the determination of the radiance clear sky surfaces and the radiance cloudy sky, the net effect on the estimated optical depths compensate.

[32] The optical depth can also be retrieved using the cloud water measurement performed by FISH. The raw data from FISH are first corrected for the oversampling of particles by dividing the fraction of the signal due to the particles by a factor of 5. The optical depth is related to the total column ice water path (IWP expressed in g $m^{-2}$) through the following expression:

$$\tau = \beta \times \mathrm{IWP} \quad (3)$$

where $\beta$ is the broadband absorption coefficient [*Starr and Cox*, 1985]. We assumed the value $\beta = 0\ 048\ m^2g^{-1}$ obtained using the formulas described by *Ebert and Curry* [1992] and assuming a size distributions with particle mode around $r \approx 5-6\ \mu m$ and particle number densities of $6-9\ L^{-1}$ for $r > 3\ \mu m$ which was measured by FSSP-300 in thin cirrus clouds at the tropopause observed during following flights.

[33] The Falcon and the Geophysica followed the same path, so the geometric parameters of the layer could be detected. From 0°S to 2°S, the layer was at a constant altitude of 18 km with a geometric thickness of approximately 1 km. We focus our attention on the portions of the flight, during which the Geophysica traversed the cloud layer, retrieving the total column ice water path (IWP) by means of FISH. The midcloud average temperature measured in situ by the Geophysica was equal to −86°C. We have used the algorithm relative to the points of the Meteosat images in which the Geophysica crossed the cloud layer, assuming midlevel clouds to be absent. The in situ observation (FISH) is compared with the satellite analysis in Table 1.

[34] The water path (i.e., optical depth) measured in situ by FISH in the cloud layer was comparable with the estimate based on the Meteosat image, using the algorithms described above. This means that the radiance observed by Meteosat can actually be ascribed to the presence of this cloud layer with the features (i.e., optical depth, altitude) observed by the aircraft. In conclusion, the direct informa-

**Table 1.** Comparison of Optical Depths Estimated From the Meteosat Data and the FISH In Situ Measurements for the Two Cloud Crossing Points Shown in Figure 5a

| Latitude, °S | Longitude, °E | Meteosat Rad., $Wm^{-2}sr^{-1}$ | Meteosat Optical Depth | FISH Optical Depth |
|---|---|---|---|---|
| −1.12 | 51.2 | 10.5 | 0.044 | 0.038 |
| −1.6 | 51.6 | 10.6 | 0.039 | 0.044 |

tion retrieved by the two aircraft and the Meteosat observations confirm the scenario that high clouds at the tropopause were present at altitudes much higher than those of the cumulus convection, which did not reach altitudes above 12 km (i.e., remained 6 km below the observed Ci). The effective emissivity of the cloud layer was very small, ranging from 0.068 to 0.061 for the two cases, respectively. From these values it can be determined that the visible optical depth at 532 nm results ranges from 0.088 to 0.078. From MAS we can retrieve a total backscatter coefficient, integrated over altitude, of $7.5 \times 10^{-4}$ 1/sr and $6 \times 10^{-4}$ 1/sr for traversing the cloud. Thus, for this cloud, we obtain an extinction/backscatter ratio approximately equal to 117–130 sr. Similar values have been found in the past by lidar observation [*Sassen and Cho*, 1992] for extremely high and cold clouds, as well as by laboratory tests [*Sassen and Lou*, 1979]. These values are comparable with those obtained in a cloud chamber by ice crystals shapes corresponding to small plates and columns. In situ observations performed by *Heymsfield* [1986] in a cirriform cloud at −83°C revealed such crystals shapes (amongst others). Applying these values of the lidar ratio to the OLEX data we can evaluate the optical depth of the cloud along all its structure, see Figure 4c. This indicates that the thinner parts of the cloud, where the large particle may already have sedimented out, have an optical depth around 0.012, which is below the threshold for visibility defined by *Sassen and Cho* [1992].

### 4.2. Generalization for the Western Indian Ocean

[35] We tried to generalize the local, in situ, observations to a larger region. For this purpose we used a qualitative method based on the Meteosat 5 IR and WV images by applying the Szejwach method. This qualitative method allows one to recognize the signature of a high cirrus cloud in the Meteosat images assuming that the radiative properties are uniform and similar to the cirrus observe during the flight.

[36] *Szejwach* [1982] describes a method for determining the temperature of semi-transparent cirrus clouds from the infrared radiances (namely the window channel and the water vapor absorption channel) measured by Meteosat. This method is based on the combination of WV and thermal IR channels through a bi-dimensional histogram, which is used to extrapolate the cloud top temperature for semi-transparent cirrus [*Desbois et al.*, 1982]. This method cannot be applied for cloud thickness below 0.0145 in the IR (approximately 0.03 in the visible range) because the cloud signature will be lost in the background fluctuations. This threshold value has been obtained from Figure 6 considering IR values that are 3 standard deviations above the mean of the background values.

[37] We have considered for these two channels an area of 100 × 13 pixel (approximately 500 × 65 km) as indicated in the box 2 reported in Figure 1 which should contain the high cloud measured by the M-55 Geophysica. The corresponding bidimensional histogram is reported in Figure 6; on the same figure we report a curve function (F(T)) that associates the temperature of a blackbody to a radiometric value (expressed in digital counts) in the IR and WV channel. Two clusters of points can be identified, one corresponding to the background conditions and the other to a thinner structure whose the max radiance in the IR channel is similar to the values reported in Table 1. For this second cluster we have calculated a regression line. The intersection of this line with the curve F(T) gives a good approximation of the temperature of the upper cloud surface [*Szejwach*, 1982]. The temperature obtained with this method is about −87 to −88°C, very close to the actual midcloud temperature measured by the aircraft (−86°C). Unfortunately for the second cluster, the number of points is so small that a regression line drawn through it would be unreliable due to the high uncertainty. For this reason this method cannot be applied in a direct way. In any case, Figure 6 demonstrates that the radiances observed in the IR and WV channels for cluster 2 are not incompatible with the observation of a single thin cloud at −86°C. These IR and WV radiance values may be combined in order to get the signature of the presence of the thin cirrus in the Meteosat 5 images.

[38] In Figure 6 we report the WV radiance values corresponding to the IR radiance measured for the thin cirrus cluster assuming it related to a thin cirrus at −86 C. These radiances will be used to extrapolate the presence of the high cirrus in the Meteosat 5 images. In Figure 7, we report an IR image where the pixels in blue indicate an IR radiance and a WV radiance corresponding to the presence of the thin layer at the tropopause (i.e., cluster 2 in Figure 6). Despite the approximations applied in its derivation, this figure mirrors the possible position and advection of a cloud layer at the tropopause in comparison with the Cb clusters

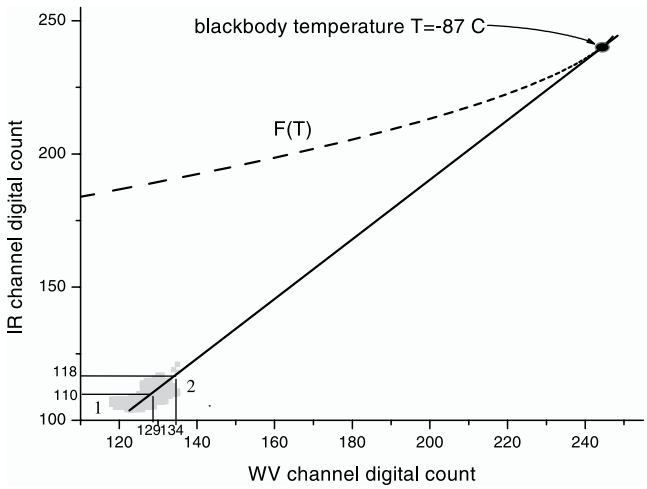


**Figure 6.** WV and IR bidimensional histogram considering an area of 130 × 30 pixels where the Ci cloud has been observed. In the same figure we also report a curve function that associates the temperature of a blackbody with a radiometric value, and we report the interpolating line of the cluster 2 points. See text for details.

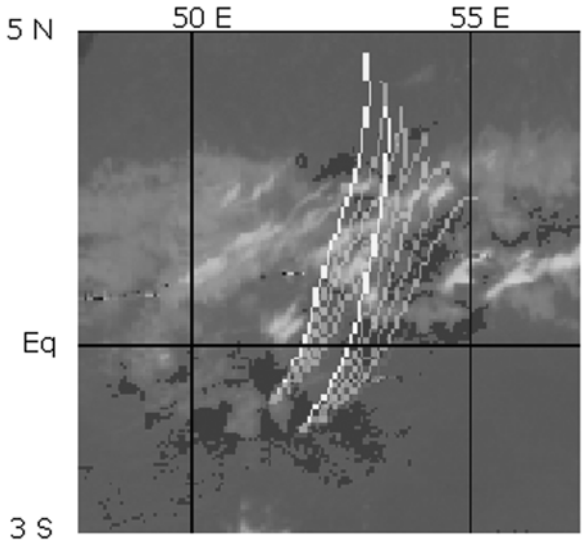


**Figure 7.** Detailed view of Figure 1. Blue regions: clouds located at the tropopause, assuming the radiative properties reported in Table 1. Colored lines: 24 hour isentropic backward trajectories (380 K, yellow; 382 K, pink; 384 K, light blue; 386 K, red; 388 K, green; and 390 K, blue) terminating at the points indicated in Table 1 where the aircraft crossed the layer. This indicates that the air masses with observed cirrus clouds originated above the Cbs cluster area (whitish regions). See color version of this figure at back of this issue.

area assuming that it has IR and WV radiances compatible with that derived from Figure 6.

[39] Three different clouds systems can now be identified in the Meteosat image. The bright white represents Cbs tops at or below the 200-mbar level; the grey represents a stratiform low-level cloud system below the 500-mbar level; and blue represents the thin high clouds located, according to the lidar observations, at or slightly below the tropopause (around 75 mbar). The high clouds (blue) can be identified only by a combination of the Meteosat and the in situ observations. The generalization to regions without in situ measurements (i.e., away from the flight path) is permissible only when the following two criteria are satisfied: (1) no clouds are present at lower altitudes (such as the stratiform clouds observed in parts of the region), and (2) the cloud optical thickness is not too small (with respect to the Meteosat sensitivity). It can be observed that the thin tropopause clouds extended to the southwest from the region with cumulus activity. According to Figure 3 this requires that they were formed above the Cb region and advected to the southwest by the upper level winds, while the Cb/Cu activity was advected into the opposite direction (see Figure 1).

[40] Figure 7 also shows, for the two crossing points, the 24-hour isentropic back trajectories between 380 K and 390 K (cloud altitude), calculated from the ECMWF analysis, terminating where the Geophysica in situ instruments detected the cirrus. Since the region of convective activity was reasonably stationary in the 24 hours prior to the flight (Meteosat images, not shown), Figure 7 shows that the air masses of interest crossed the region with the mesoscale convective clusters. In Figure 8 we report the IR thermal brightness temperature history along the back trajectory followed by the air mass at 384 K (close to cloud center) ending at the observation point. Before crossing the Cb area on day number 50 (roughly half a day before the observation) the IR thermal brightness temperature of the column still was close to the background value and well above the radiance value observed in the presence of the thin cirrus clouds. Hence, it is likely to assume that before crossing the Cb area on day number 50 the cirrus was not yet present in the air masses where it was observed. Furthermore, the same air masses have not encountered any Cb with a cloud-tops getting anywhere near the tropopause altitude. The observed cirrus cannot, therefore, be considered a Cb anvil. In fact, if it was generated by a deep convection encountered before the two days trajectory reported in Figure 8, the optical depth should be higher than the observed one (assuming that anvils optical depth decreases with increasing the distance from the originating convection [*Ackerman et al.*, 1988]), and hence the IR brightness temperature before day number 50 should be lower than the observed one certainly well below the background value reported in Figure 8.

[41] Conversely, the convective area crossed half a day before the observation corresponds to the Cb cluster region described above. It is much lower than the cirrus, but obviously responsible for its formation. This observation appears to be different from those described by *Pfister et al.* [2001], according to which cirrus with scattering ratios similar to the one described here are considered to be Cb anvils.

## 5. Humidity Measurements Across the Cirrus Layer

[42] The tropical upper troposphere is often very close to the saturation level with respect to ice [*Jensen et al.*, 1999; MacKenzie et al., manuscript in preparation, 2002; Luo et al., submitted manuscript, 2002]. Of course, these are very favorable conditions for cirrus formation and maintenance. In the following, we ask how this high relative humidity can be established.

### 5.1. Evidence for a Vertical Mixing Barrier

[43] In Figure 9 we report the in situ chemical and aerosol measurements taken on board the Geophysica across the cloud layer. This plot has been obtained by using the water vapor measured by FLASH (i.e., the Ly-$\alpha$ hygrometer which measures only the gas phase water and does not sample particles) (Figure 9a), the temperature (Figure 9b) and the zonal and meridional wind (Figure 9d) measured by the sensors on board of the Geophysica, the aerosol backscattering profiles obtained using the MAS data (Figure 9b), and the ozone measurements performed by FOZAN (Figure 9c). Furthermore, also the Richardson number (Figure 9e) has been calculated using the following formula:

$$Ri = \frac{g/\theta_v * \partial\theta_v/\partial z}{\left[\left(\frac{\partial U}{\partial z}\right)^2 + \left(\frac{\partial V}{\partial z}\right)^2\right]} \quad (4)$$

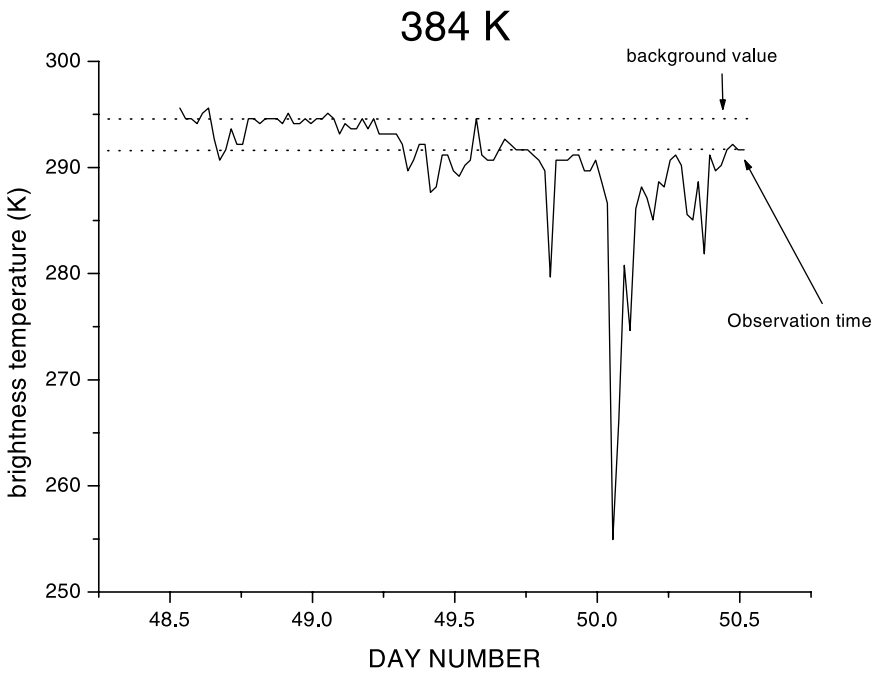


**Figure 8.** Thermal IR brightness temperature calculated from the Meteosat 5 observations along the backward trajectory (at 384 K) of the air mass terminating at the crossing point of the Geophysica flight path with the thin cirrus at the tropopause (pink trajectory ending at 1.6°S in Figure 6). Before traversing the convective area (half a day before the observation), the radiance of the column was around the background value, excluding the presence of a thin cirrus.

Theoretical and laboratory research suggest that a laminar flow becomes unstable and the onset of turbulence when Ri is smaller then the critical Richardson number Rc. When a flow is turbulent then another value Rt indicates the termination of turbulence. Summarizing a laminar flow becomes turbulent when Ri < Rc and a turbulent flow becomes laminar when Ri > Rt. According to the existing literature, it appears that $R_c = 0.25$ and $R_t = 1.0$ work fairly well. These threshold values are reported in Figure 9e together with the Richardson profile.

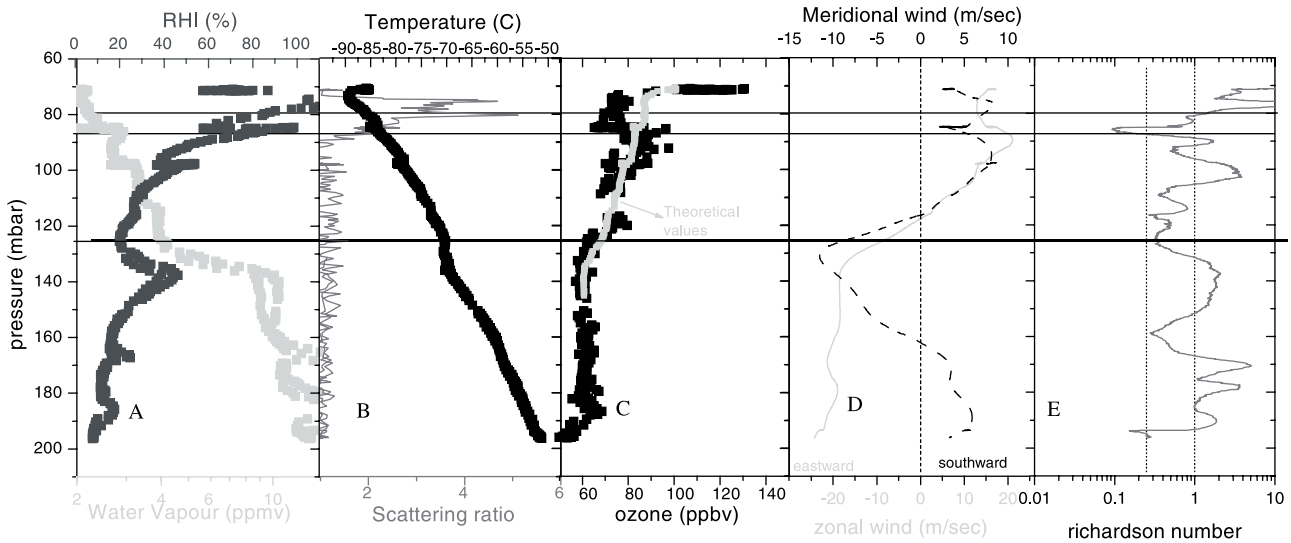


**Figure 9.** (a) Water vapor profile reported as relative humidity with respect to ice (RHI) and as mixing ratio retrieved from FLASH. (b) Temperature and MAS aerosol backscattering ratio. (c) ozone mixing ratio as measured by FOZAN and theoretical value (green line), (d) zonal and meridional wind as measured by the Geophysica, and (e) Richardson number with two thin horizontal lines indicating the possible presence of turbulence. The thick horizontal line at 125 mbar indicates the altitude reached by convective activity in the area.

[44] According to the wind direction these profiles represent a combination of air masses coming form different direction at different altitudes. In particular only the air masses, at 70–80 mbar where the cirrus is detected, are downwind to the convective cluster area. The rest of the profile is representative of air masses not perturbed by the same convective region.

[45] A sharp decrease in the $H_2O$ mixing ratio is detected at about 130 mbar accompanied by an isothermal layer in the temperature profile, which indicates suppressed vertical mixing. This altitude of the isothermal layer is equivalent to the limit reached by the deepest tropical convection that we were able to find in the western Indian Ocean. For example, on 24 February, i.e., five days after the flight discussed here, the Geophysica sampled ice particles at the upper edge of Cb turrets reaching 15 km altitude, corresponding to about 130 mbar. Meteosat observations taken at regular intervals (not shown) reveal a strong and extended region of convection in the southwest sector close to Madagascar. Pressures of the upper cloud edges of this convective activity can be estimated to be close to 14 km. It is likely that this continuous activity has transported large amounts of water vapor from the low troposphere to altitudes up to 130 mbar, and that the result of this deep convection is found in the profiles reported in Figure 9, with the limit in the vertical mixing associated with this convection around 130 mbar.

[46] Above 130 mbar, several secondary peaks in the water vapor profiles are detected, again accompanied by thin inversion layers in the temperature profile. A minimum $H_2O$ mixing ratio in the gas phase of about 2 ppmv is detected around the tropopause. Taking into account the cloud condensed water content of 1.8–2.2 ppmv measured by FISH, the total water content at the tropopause is about 3.8–4.4 ppmv. The overall accuracy of this instrument is 6%; the precision is approximately 0.15 ppmv.

[47] The relative humidity profile shows an increase with altitude, reaching high value of supersaturation (140%) at the tropopause. It is clear that directly below the tropopause, where the clouds are observed, the atmosphere must at least be saturated with respect to ice. In fact, supersaturation is detected at the cloud top, whilst the lower part of the cloud is located in a subsaturated environment. This is very similar to what we found in the vicinity of ultrathin tropopause clouds (Luo et al., submitted manuscript, 2002).

[48] Hence, the water profile indicates that the air masses are firstly strongly dehydrated across the lower limit of the TTL, but only reach their minimum water vapor content at the tropopause.

[49] Above the isothermal layer in Figure 8 there is an increase in the ozone mixing ratio, which also indicates the presence of an intermediate chemical transition zone. This is similar to the one reported by *Folkins et al.* [1999], between 130 mbar and the tropopause which assume a slow ascent in the tropopause layer assuming a calculated heating rate 0.5 K/day and an ozone in situ production rate of 5 ppb/day, in the Figure 9c the green curve represents the theoretical values obtained by using a balance between ozone in situ production and up welling described by *Folkins et al.* [1999]. Comparing the two curves a general accordance between the values measured and those estimated is observed for altitudes above the 130 mbar.

[50] The only discrepancy is observed around 80 mbar (at the altitudes where the cirrus has been detected), where the ozone measured is lower than the expected curve produced theoretically. In fact, the values measured are lower and similar to those observed at 105–110 mbar. The higher ozone mixing ratio values observed at 90 mbar is similar to the value expected assuming a balance between the ozone production and a slow upwelling, so we suppose that the minima at 80 mbar cannot be ascribed to rich ozone stratospheric midlatitude intrusion at lower altitudes.

### 5.2. Discussion of a Possible Ci Formation Mechanism

[51] The brightness temperature calculated along the backtrajectories in Figure 8 suggests that the cirrus cloud has not been advected from other regions (i.e., Micronesia region) but, rather, has been generated locally over the western Indian Ocean. Furthermore, we found an extremely high, cold, and relatively humid tropopause in the region of the cirrus cloud.

[52] As stated above, both the RHI profile above 130 mbar [*Jensen et al.*, 1999], and the ozone mixing ratio profile, could be the consequence of slow ascent in the tropopause, assuming heating rates well below 1K/day (a value around 0.5 K/day has been assumed from the ozone profile). Discrepancies (ozone minimum and supersaturation in the RHI) are observed just below the tropopause level where the Ci layer is detected.

[53] Which specific mechanism could have triggered such high relative humidities in the tropopause layer, the formation of the thin cirrus at the tropopause, and the corresponding minimum in the ozone profile above the convective region?

[54] As suggested by *Churchill and Houze* [1990, 1984a], humid air masses may be lifted when they reach a convective system. According to this hypothesis, *Jensen et al.* [1996b] have formulated a cirrus formation mechanism triggered by slow vertical motion or turbulent mixing. In their model they assumed a moist layer just below the tropopause (from 15.5 to 17 Km) with an RHI equal to 95%. The Ci formation is triggered by an updraft in the last 1.5 km of the troposphere with a peak velocity of 1 cm-s-1. They estimated according to their simulation that the Ci cloud persisted for hours even when the updraft decreased after 10 hours. Alternatively, they indicated that also turbulent mixing can drive the Ci formation producing a mixed layer where the mixing ratio is constant and thus with the upper part supersaturated with respect to ice and the lower part drier. Furthermore, they stated for this turbulent case, that the number of ice crystal nucleated is probably higher than the slow uplift scenario.

[55] Bearing in mind that only the upper part of the profiles reported in Figure 9 are representative of the cluster area above which we supposed the Ci formed, we tried to understand which could have been the triggering mechanism.

[56] The mesoscale undulations over a convective cluster associated with upward propagating gravity waves would uplift the tropopause, but it would be essentially an isentropic process and thus when the activities are damped the air should return to the original altitudes and the Ci particles should evaporate. Also the peak vertical wind speed as captured by the ECMWF analysis data above the convective

cluster is about 5 mm $s^{-1}$ lower than the values used in the simulation described above. Thus, taking into account the observation performed, this first scenario for the cloud nucleation appears to be very unlikely.

[57] Can on the other hand the turbulent mixing be responsible for the Ci formation?

[58] Using measurement performed in the CEPEX campaign, *Teitelbaum et al.* [1999] have reported mixed layers induced by convectively generated gravity waves. These mixing layers were traced by constant values in the ozone mixing ratio and potential temperature profiles. In the cases reported by *Teitelbaum et al.* [1999], a mixed layer started from the critical layer and extended up to 2 km above.

[59] Taking into account the wind profiles reported in Figure 9, and assuming them to be valid also for the convective area, we have retrieved the critical levels assuming convectively generated waves propagating upwards. The critical level represents the altitude at which the vertical wavenumber is infinite.

[60] The vertical wavenumber ($m$) has been calculated using the following formula [*Piani et al.*, 2000]:

$$m = \sqrt{\frac{N^2}{(c_x - U)} - \kappa^2} \tag{5}$$

where N is the buoyancy period; U is the storm-relative zonal wind $c_x$ is the group velocity, and $\kappa$ is the horizontal wavenumber.

[61] Past observation of gravity waves [*Pfister et al.*, 1993], have shown that the gravity waves cannot be considered in term of linear, stationary wave dynamics. Their analysis of a case study during the STEP campaign suggests that they may be moving at about 4 $ms^{-1}$. In the same study a value of $\kappa = 5.7 \times 10^{-5}$ $m^{-1}$ has been considered.

[62] Using these values in equation (5) we obtain that the critical level is located at 110 mbar (roughly 16 km) (figure not shown).

[63] Considering a mixed layer up to 2 km (as observed by *Teitelbaum et al.* [1999]) started from this altitude, the ozone mixing ratio would be well mixed from 110 mbar up to roughly 78 mbar. Thus above the convective cluster the ozone mixing ratio would be mixed within this altitude range, which is consistent with a net upward flux of water vapor due to turbulence acting on a background of decreasing water vapor with height and increasing ozone with height.

[64] This hypothesis of net transport of lower altitude (110 mbar) air to the tropopause is supported by Figure 9c, where we report the ozone profile measured by FOZAN, and a minimum corresponding to presence of the cloud layer is observed. The ozone values observed at the tropopause are as low as those observed at altitudes around 110 mbar and comparing this profile with other taken in an unperturbed region on the same day it appears that the ozone at the tropopause is lower than in unperturbed cases. According to the discussion reported above, it is possible to explain this ozone minimum at the tropopause as midtropospheric air masses (110 mbar) which, in the area where the moderate Cbs are detected, have been lifted probably by vertical diffusion as a consequence of the mixing layer from around 110 mbar to the tropopause, thereby modifying the ozone (and water vapor) profile at the tropopause. This may have been caused by Cb-induced wave activity, which modifies the structure of the TTL.

[65] Likely the turbulence induced by the mixing layer could have been responsible for the cloud formation. In fact, as stated by *Jensen et al.* [1996b], water vapor would have been transported at high altitudes by vertical diffusion producing super saturation at higher altitudes inside the mixed layer. As a matter of fact like in the case of the ozone mixing ratio profile the total water (condensed and gas phase) just below the tropopause is very close to the total water content (only gas phase) observed around 110 mbar.

[66] In Figure 9e we have calculated also the Richardson number, which indicates that in the lower part of the cloud (as indicated by the horizontal lines), the presence of turbulence is highly probable. This portion of the Ri profile can identify the turbulent region, which is between the critical Richardson number $R_c$ and the value $R_t$, indicating the start and the end of turbulence. This turbulence may be either a residual of the turbulence induced by the critical level, assuming that long wave radiation would cool the upper part of the cloud damping the turbulence in the upper part of the cloud, or a consequence of the long wave heating of the low part of the clouds which could produce the observed turbulence. According to *Teitelbaum et al.* [1999], the former case is a realistic possibility, but we have not direct information obtained above the convective area, so we can only speculate, using the ozone mixing ratio profiles and the possible cirrus formation mechanisms existing in the literature.

[67] The net water vapor updraft induced by the turbulence would have created favorable conditions for the formation of cirrus through the in situ nucleation of ice crystals [*Jensen et al.*, 1996b]. Subsequent horizontal advection due to the upper level winds could explain how the location of the observation (cirrus and supersaturated air masses) is shifted to the southwest relative to the convective area [*Jensen et al.*, 1994]. This data set also supports the *Teitelbaum et al.* [1999] study about mixing layers induced by the gravity waves, and extends the conclusion of *Teitelbaum et al.* [1999] by showing that absorbed gravity waves could also have a role into the formation of thin cirrus at the tropopause, without the necessity of having strong Cbs overshooting the TTL region.

## 6. Conclusions

[68] During the first flight of APE-THESEO, a thin cirrus, with a relatively high optical thickness of 0.1, was observed. The lidar ratio, estimated by using the LIDAR data together with the thermal IR Meteosat radiances, was equal to 117–130 sr. This value is compatible with cloud particles composed of small plate-like, or cylindrical, ice crystals. Apparently, this observation is different from those reported by *Pfister et al.* [2001]. In fact, it is not easy to fit this Ci into the classification they have indicated according to the Ci near the tropopause observed during the TOTE/VOTE campaign. According to its high altitude, the present cloud should belong into class II cirrus clouds. However, it was not found directly downstream of deep convection. Rather, we have shown that the present Ci cannot be

considered to be anvil outflow, because of the low altitude reached by the Cbs in the western Indian Ocean at this time. A first strong decrease in the water vapor content is observed across the lower limit of the TTL at 14–15 km, followed by a slower decrease and a minimum at the tropopause. The dehydration potential of the observed Ci is high. We have measured roughly 2 ppmv (at 18 km) of water condensed in the cloud particles. Simple microphysical argumentation, based on T-matrix computations, suggests that the observed ice particles had an average radius around 5 μm and were aspherical, with an aspect ratio ranging from 0.5 to 0.7 (Luo et al., submitted manuscript, 2002), in agreement with cold cirrus cloud observations reported by *Heymsfield* [1986]. This implies a sedimentation speed of about 1 km in 24 hours.

[69] These observed Ci are extremely cold, and their potential impact on radiative transfer may not be negligible. The estimated effective emissivity retrieved by Meteosat in the thermal IR channel is of the order of 0.068 and, the surface radiance in the area is equal to 11.6 $Wm^{-2}sr^{-1}$, but the IR thermal radiance emitted in space was reduced, according to Table 1, by 10%.

## 7. Suggested Interpretations

[70] In this study we have described a data set, which is important in the context of the current discussion on formation and maintenance of cirrus clouds at the tropical tropopause. Unfortunately the collected data are not enough for a complete and clear analysis, so only interpretation based on the most likely explanation can be performed using the existing literature and recent studies in this field.

[71] In this section we summarize our speculations.It is very likely that the thin cirrus was formed above the Cbs, as has been observed in the past [*Harris-Hobbs et al.*, 1990; *Churchill and Houze*, 1984b]. According to the existing literature describing the mechanism of cirrus formation, we suggest that the cirrus observed is most likely generated by a net water vapor transport, possibly consequence of a turbulence layer induced at the critical levels by inertia-gravity waves generated by the convective system at middle altitudes.

[72] The mechanism of high-altitude Ci formation corroborates the new paradigm of a tropical tropopause layer (TTL) [*Sherwood and Dessler*, 2000] or "substratosphere" [*Thuburn and Craig*, 2000], which is decoupled from the convection-dominated lower troposphere. The formation of cirrus, observed during the flight described in this paper, is therefore a consequence of local activity in the area of the western Indian Ocean, and does not require tropopause-penetrating Cbs.

[73] This mechanism could have a significant impact on the water vapor distribution in the tropical upper troposphere, although this remains to be tested.

[74] Furthermore, the radiative heating in the cloud could drive a local temperature increase combined with upward motion of the cloud and turbulent motions in the cloud [*Rosenfield et al.*, 1998]. This implies that cirrus at the tropopause could affect the lower stratospheric circulation through an upward vertical motion driven by diabatic heating [*Gage et al.*, 1991]. These effects depend strongly on the horizontal scale of the cirrus and on the temperature lapse rate at the tropopause [*Jensen et al.*, 1999]. While the magnitude of the radiative effect of this thin cirrus at the tropopause is locally very small when compared to thicker cirrus cloud, taking into account their high aerial coverage and relatively high stability, they may significantly perturb the heat budget near the tropopause.

[75] Finally, thin cirrus at the tropopause can act as a precursor of the subvisible cirrus observed very often during APE-THESEO, and in particular also of the ultrathin tropical tropopause clouds described by Luo et al. (submitted manuscript, 2002).

[76] **Acknowledgments.** This research has been performed in the frame of the APE-THESEO project supported by EU contract ENV4CT970533, by the Italian Space Agency, by the U.K. NERC UTLS Ozone Programme, by the German Bundesministerium für Bildung und Forschung within contract 01 LA 9829 and by INTAS grant YSF00-231. The authors wish to thank the ECMWF for the meteorology data provided through the NILU data center, EUMETSAT for the assistance provided during the campaign and for the availability and the decryption of Meteosat 5 high-resolution data used in this paper, and the U.K. Met Office, in particular Peter Salter and Ian Cameron, for their professional and fundamental meteorological support provided during the campaign. We thank Boris Lepukhov for in situ meteorological data measured by the M-55 Geophysica. Furthermore, both the Geophysica and Falcon airplane team, and in particular the pilots, are greatly acknowledged. Finally, the authors wish to thank Gilbert Faure, Alain Volcere and all the personnel of the directorate of Seychelles civil aviation for their assistance and support provided during the campaign.

## References

Ackerman, T. P., et al., Heating rates in tropical Anvils, *J. Atmos Sci.*, *45*, 1606–1623, 1988.

Adriani, A., M. Viterbini, F. Cairo, S. Mandolini, and G. Di Donfrencesco, Multi wavelength Aerosol Scatterometer for airborne experiments to study the stratospheric particle optical properties, *J. Atmos. Oceanic Technol.*, *16*, 1328–1335, 1999.

Boehm, M. T., and J. Verlinde, Stratospheric influence on upper tropospheric tropical cirrus, *Geophys. Res. Lett.*, *27*, 3209–3212, 2000.

Brewer, A. W., Evidence for a world circulation provided by the measurements of helium and water vapour distribution in the stratosphere, *Q. J. R. Meteorol. Soc.*, *75*, 351–363, 1949.

Browell, E. V., A. F. Carter, S. T. Shipley, R. J. Allen, C. F. Butler, M. N. Mayo, J. H. Siviter Jr., and W. M. Hall, NASA Multipurpose Airborne DIAL system and measurements of ozone and aerosol profiles, *Appl. Opt.*, *22*, 522–534, 1983.

Churchill, D. D., and R. A. Houze, Mesoscale updraft magnitude and cloud ice content deduced from the ice budget of the stratiform region of a tropical cloud cluster, *J. Atmos. Sci.*, *41*, 1717–1725, 1984a.

Churchill, D. D., and R. A. Houze, Development and structure of winter monsoon cloud cluster on 10 December 1978, *J. Atmos. Sci.*, *41*, 933–960, 1984b.

Churchill, D. D., and R. A. Houze, Radiatively driven stratosphere-troposphere interaction near the tops of tropical cloud clusters, paper presented at Conference on Cloud Physics, Am. Meteorol. Soc., San Francisco, Calif., 1990.

Danielsen, E., A dehydration mechanism for the stratosphere, *Geophys. Res. Lett.*, *9*, 605–608, 1982.

Desbois, M., G. Seze, and G. Szejwach, Automatic classification of clouds on Meteosat imagery: Application to high level clouds, *J. Appl. Meteorol.*, *21*, 401–412, 1982.

Ebert, E. E., and J. A. Curry, A parametrization of ice cloud optical properties for climate models, *J. Geophys. Res.*, *97*, 3831–3836, 1992.

Folkins, I., M. Lowenstein, J. Podolske, S. J. Oltmans, and M. Proffitt, A barrier to vertical mixing at 14 km in the tropics: Evidence from ozonesondes and aircraft measurements, *J. Geophys. Res.*, *104*, 22,095–22,102, 1999.

Gage, K. S., J. R. McAfee, D. A. Carter, A. C. Riddle, G. C. Reid, and B. B. Balsley, Long term mean vertical motion over the tropical Pacific: Wind profiling Doppler radar measurements, *Science*, *254*, 1771–1773, 1991.

Harris-Hobbs, R., D. Rusk, M. Bradford, and D. R. Booker, HAT cirrus notes and observation, U.S. Army Strategic Command, Huntsville, Ala., 1990.

Heymsfield, A. J., Ice particles observed in a cirriform cloud at −83 C and implication for polar stratospheric clouds, *J. Atmos. Sci.*, *43*, 851–855, 1986.

Holton, J. R., P. H. Haynes, M. E. McIntyre, A. R. Douglass, R. B. Rood, and L. Pfister, Stratosphere-troposphere exchange, *Rev. Geophys.*, *33*, 403–439, 1995.

Houze, R. A., Observed structure of mesoscale convective systems and implications for large scale heating, *Q. J. R. Meteorol. Soc.*, *115*, 425–432, 1989.

Jensen, E. J., O. B. Toon, D. L. Westphal, S. Kinne, and A. J. Heymsfield, Microphysical modelling of cirrus, 1, Comparison with 1986 FIRE IFO measurements, *J. Geophys. Res.*, 10,421–10,442, 1994.

Jensen, E., O. W. Toon, L. Pfister, and H. B. Selkirk, Dehydration of the upper troposphere and lower stratosphere by subvisible cirrus clouds near the tropical tropopause, *Geophys. Res. Lett.*, *23*, 825–828, 1996a.

Jensen, E. J., O. B. Toon, H. B. Selkirk, J. D. Spinhirne, and M. R. Schoeberl, On the formation and persistence of subvisible cirrus clouds near the tropical tropopause, *J. Geophys. Res.*, *101*, 21,361–21,375, 1996b.

Jensen, E. J., W. G. Read, J. Mergenthaler, B. J. Sandor, L. Pfister, and A. Tabazadeh, High humidity and subvisible clouds near the tropical tropopause, *Geophys. Res. Lett.*, *26*, 2347–2350, 1999.

Johnson, R., and D. Kriete, Thermodynamic circulation characteristics of the winter monsoon tropical mesoscal convection, *Mon. Weather Rev.*, *110*, 1898–1911, 1982.

Liou, K. N., On the radiative properties of cirrus in the window region and their influence on remote sensing of the atmosphere, *J. Atmos. Sci.*, *31*, 522–532, 1974.

McFarquhar, G. M., A. Heymesfield, J. Spinhirne, and B. Hart, Thin and subvisible tropopause cirrus: Observations and radiative impacts, *J. Atmos. Sci.*, *57*, 1841–1853, 2000.

Merkulov, S., and V. Yushkov, Some results of aircraft stratospheric water vapor measurement in the arctic polar vortex (in Russian), *Meteorol. Hydrol.*, *7*, 107–113, 1999.

Nee, J. B., C. N. Len, W. N. Chen, and C. I. Lin, Lidar observation of the cirrus cloud in the tropopause at Chung-Li (25°N, 121°E), *J. Atmos. Sci.*, *55*, 1977–1996, 1998.

Newell, R. E., and S. Gould Stewart, A stratospheric fountain?, *J. Atmos. Sci.*, *38*, 2789–2795, 1981.

Pfister, L., K. R. Chan, T. P. Bui, S. Bowen, M. Legg, B. Gary, K. Kelly, M. Proffitt, and W. Starr, Gravity waves generated by a tropical cyclone during the STEP tropical field program: A case study, *J. Geophys. Res.*, *98*, 8611–8638, 1993.

Pfister, L., et al., Aircraft observations of thin cirrus clouds near the tropical tropopause, *J. Geophys. Res.*, *106*, 9765–9786, 2001.

Piani, C., D. Durran, M. J. Alexander, and J. R. Holton, A numerical study of three dimensional gravity waves triggered by deep tropical convection and their role in the dynamics of the QBO, *J. Atmos. Sci.*, *57*, 3689–3702, 2000.

Platt, C. M. R., S. A. Young, P. J. Mason, G. R. Patterson, S. C. Marsden, and R. T. Austin, The optical properties of equatorial cirrus from observation in the ARM pilot radiation observation experiment, *J. Atmos. Sci.*, *55*, 1977–1996, 1998.

Potter, B., and J. Holton, The role of monsoon convection in the dehydration of the lower tropical stratosphere, *J. Atmos. Sci.*, *52*, 1034–1050, 1995.

Rosenfield, J. E., D. B. Considine, M. R. Schoeberl, and E. V. Browell, The impact of subvisible cirrus clouds near the tropical tropopause on stratospheric water vapor, *Geophys. Res. Lett.*, *25*, 1883–1886, 1998.

Sassen, K., and B. S. Cho, Subvisual-thin cirrus lidar data set for satellite verification and climatological research, *J. Appl. Meteorol.*, *31*, 1275–1285, 1992.

Sassen, K., and K. N. Lou, Scattering of polarized laser light by water droplet, mixed phase and ice clouds, II, *J. Atmos. Sci.*, *36*, 852–861, 1979.

Sherwood, S. C., and A. E. Dessler, On the control of stratospheric humidity, *Geophys. Res. Lett.*, *27*, 2513–2516, 2000.

Starr, D. O'C., and S. K. Cox, Cirrus clouds, part I, A cirrus cloud model, *J. Atmos. Sci.*, *42*, 2663–2681, 1985.

Szejwach, G., Determination of semi-transparent cirrus cloud temperature from infrared radiances: Application to Meteosat, *J. Appl. Meteorol.*, *21*, 348–393, 1982.

Teitelbaum, H., M. Moustaoui, R. Sadourny, and F. Lott, Critical levels and mixing layers induced by convectively generated gravity waves during CEPEX, *Q. J. R. Meteorol. Soc.*, *125*, 1715–1734, 1999.

Thomas, A., et al., In situ measurements of background aerosol and subvisible cirrus in the tropical tropopause region, *J. Geophys. Res.*, *107*(D24), 4763, doi:10.1029/2001JD001385, 2002.

Thuburn, J., and G. C. Craig, Stratospheric influence on tropopause height: The radiative constraint, *J. Atmos. Sci.*, *57*, 17–28, 2000.

Tsuda, T., Y. Murayama, H. Wiryosumarto, S. W. B. Harijono, and S. Kato, Radiosonde observation of equatorial atmosphere dynamics over Indonesia, 2, Characteristic of gravity waves, *J. Geophys. Res.*, *99*, 10,507–10,516, 1994.

Tuck, A. F., et al., The Brewer-Dobson circulation in the light of high altitude in situ aircraft observations, *Q. J. R. Meteorol. Soc.*, *123*, 1–69, 1997.

Winker, D. M., and C. R. Trepte, Laminar cirrus observed near the tropical tropopause by LITE, *Geophys. Res. Lett.*, *25*, 3351–3354, 1998.

Wirth, M., and W. Renger, Evidence of large scale ozone depletion within the arctic polar vortex 94/95 based on airborne LIDAR measurements, *Geophys. Res. Lett.*, *23*, 813–816, 1996.

Yushkov, V., A. Oulanovsky, N. Lechenuk, I. Rudakov, L. Stefanutti, F. Ravegnani, U. Bonafé, and T. Georgiadis, A chemiluminescent analyzer for stratospheric measurements of the ozone concentration (FOZAN), *J. Atmos. Oceanic Technol.*, *16*, 1344–1349, 1999.

Zöger, M., et al., Fast in situ hygrometers: A new family of balloonborne and airborne Lyman-$\alpha$ photofragment fluorescence hygrometers, *J. Geophys. Res.*, *104*, 1807–1816, 1999.

A. Adriani, F. Cairo, and G. Didonfrancesco, ISAC-CNR, Via Fosso del Cavaliere, 00133 Roma, Italy.

S. Balestri, APE srl, Via Jacopo Nardi 65, 50127 Firenze, Italy.

J. Beuermann and C. Schiller, Forschungszentrum Jülich, D-52425 Jülich, Germany.

R. Carla, IFAC-CNR, Via Panciatichi 64, 50127 Firenze, Italy.

C. Kiemle, Deutsches Zentrum für Luft- und Raumfahrt (DLR), Oberpfaffenhofen, 82234 Wessling, Germany.

B. Luo, T. Peter, and H. Wernli, Institute for Atmospheric and Climate Science, ETH-Hoenggerberg, CH-8093 Zurich, Switzerland.

R. MacKenzie, Environmental Science Department, Lancaster University, Lancaster, LA1 4YQ, UK.

F. Ravegnani, ISAC-CNR, Via Gobetti 101, 40129 Bologna, Italy.

G. Redaelli, Dipartimento di Fisica, Universita' Dell'Aquila, Via Vetoio, 67010 Coppito (AQ), Italy.

V. Santacesaria, Advanced Computer System SpA, Via Della Bufalotta 378, 00139 Roma, Italy.

N. Sitnikov, A. Ulanovsky, and V. Yushkov, CAO, Pervomayskaya 3, Dolgoprudny, Moscow region 141700, Russia.

L. Stefanutti, Geophysica-GEIE, Via Pancaldo 21, 50127 Firenze, Italy.

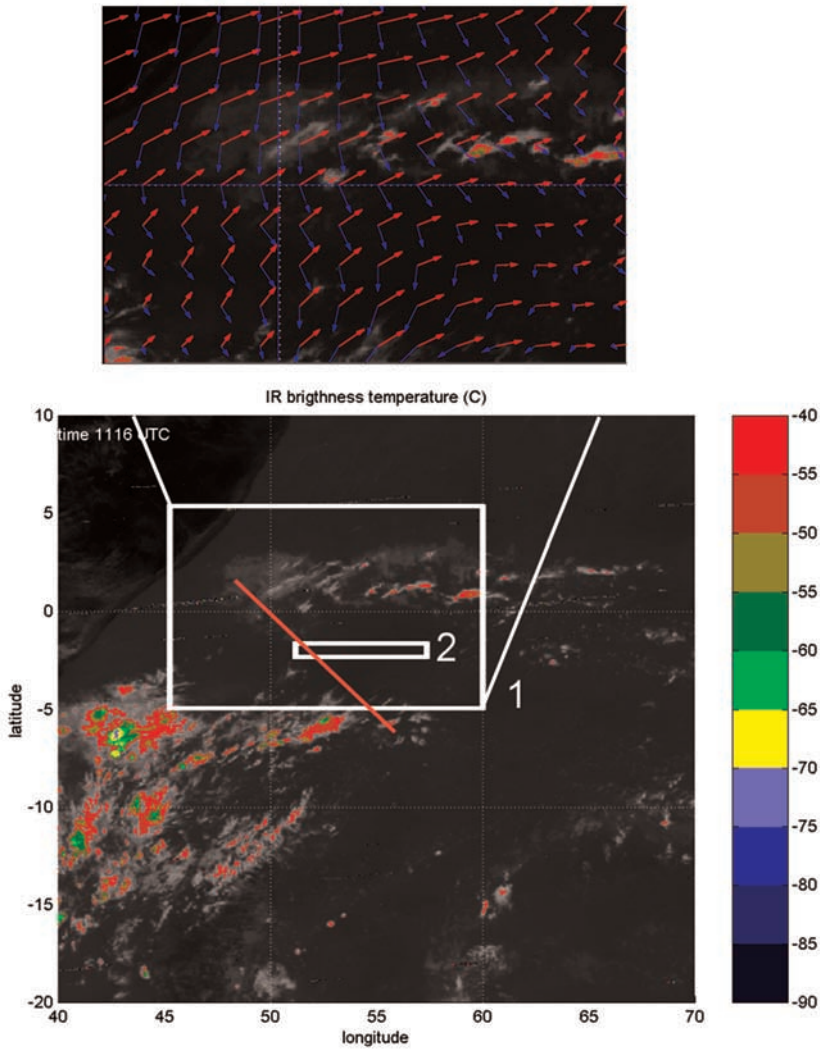


**Figure 1.** IR brightness temperature image acquired by Meteosat 5 during the APE-THESEO flight on 19 February 1999 from the Seychelles towards Mogadishu (the coastline of Somalia is visible in the upper left corner). The red line indicates the flight path of the aircraft, and the white box (box 1) indicates a region with high cirrus close to the tropopause. Included in this box is a second white box (box 2) that is considered in the analysis reported in Figure 6. The inset shows the wind field at 200 mbar (red) and 100 mbar (blue); the direction of the anvils outflow is aligned to the wind field at 200 mbar.

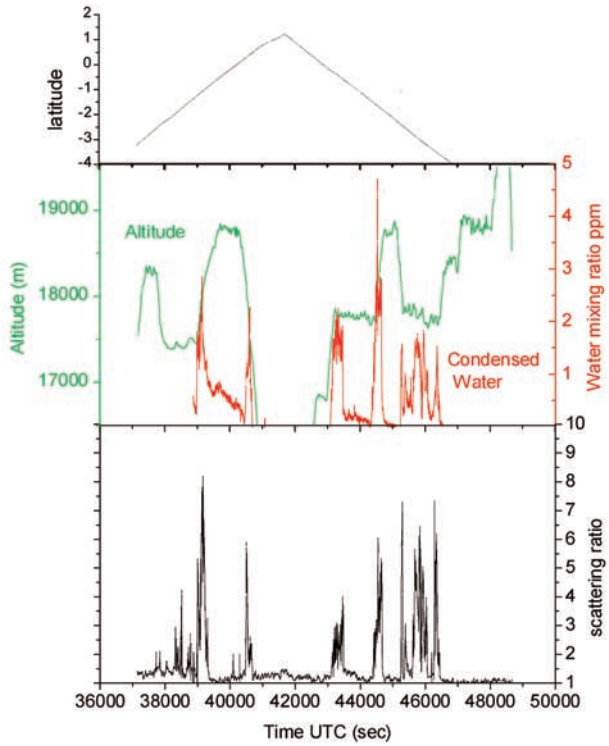


**Figure 5.** Latitudes covered (upper panel) and in situ measurements performed by the Geophysica (middle and lower panels) during the flight on 19 February 1999. Lower panel: aerosol backscattering ratio at 532 nm from MAS. Middle panel: condensed phase water mixing ratio (after subtraction of gas phase mixing ratio) and GPS flight altitude.

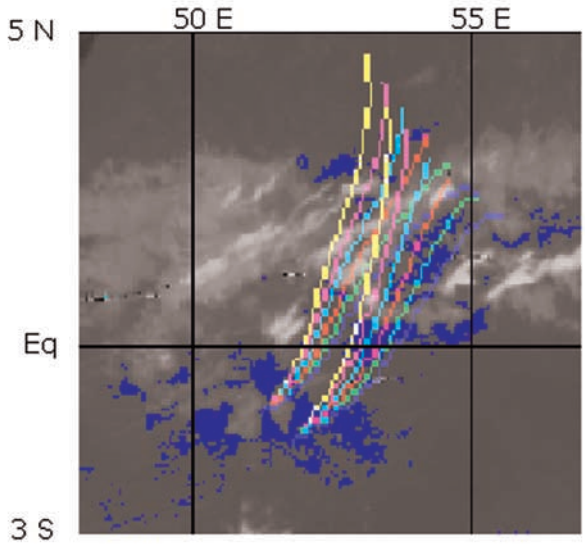


**Figure 7.** Detailed view of Figure 1. Blue regions: clouds located at the tropopause, assuming the radiative properties reported in Table 1. Colored lines: 24 hour isentropic backward trajectories (380 K, yellow; 382 K, pink; 384 K, light blue; 386 K, red; 388 K, green; and 390 K, blue) terminating at the points indicated in Table 1 where the aircraft crossed the layer. This indicates that the air masses with observed cirrus clouds originated above the Cbs cluster area (whitish regions).